

Electric-field ionization of Rydberg states of H_3

C. Bordas* and H. Helm

Molecular Physics Laboratory, SRI International, 333 Ravenswood Avenue, Menlo Park, California 94025

(Received 10 August 1992)

The stability of Rydberg states of triatomic hydrogen in an external electric field is investigated for principal quantum numbers ranging from $n=50$ to 110. When excited in the presence of an electric field, the states with an electric-field projection of the total angular momentum $M_N=0$ are found to be rapidly field ionized above the classical saddle-point energy. However, a significant proportion of the states for $M_N=1$ is observed to be stable above this threshold, with lifetimes exceeding 10^{-6} s. A perturbative treatment of the molecular Stark effect indicates that different behavior of $M_N=0$ and 1 Stark states is a consequence of the stronger coupling among the states of the $M_N=0$ manifold. Following excitation under near-zero field conditions, a predominantly diabatic evolution of the Stark manifold of H_3 is observed, for slew rates of a few times 10^7 (V/cm)/s. This behavior results from the nondefinition of the projection of the total angular momentum of the molecule excited at near-zero field, where a broad manifold of l states is prepared within the bandwidth of the laser. For a comparison, similar experiments are carried out in atomic hydrogen and helium.

PACS number(s): 33.90.+h, 32.60.+i

I. INTRODUCTION

Electric-field ionization (EFI) of Rydberg states has been widely investigated in atoms as well as in molecules. Experiments with atomic hydrogen [1,2], the prototype for all processes involving Rydberg states, confirm precisely the theoretical predictions [3–11]. Alkali-metal atoms, which in many aspects resemble atomic hydrogen, have been more widely studied [12–26], and the nonhydrogenic effects of alkali-metal atoms in EFI have been analyzed in detail. Investigations of the rare gases helium [27] and xenon [28] have also confirmed that many-electron systems behave similarly to alkali-metal atoms. Electric-field ionization of molecules has been mainly confined to the molecules H_2 [29–32], Li_2 [33–35], and Na_2 [36–38]. Some work on the polyatomic molecules naphthalene and benzene has also been reported [39].

Beyond its intrinsic interest, a motivation for studying field ionization is that it is a most sensitive and frequently used method for detection of Rydberg states of atoms and molecules. The method can also be selective, because the field-ionization threshold as well as the field-ionization dynamics depend on the binding energy of the electron [17] and vary with the m_l quantum number for a given state [16,18,23].

On the basis of the many theoretical treatments of the Stark effect in atomic hydrogen, field ionization in atoms is well understood. However, many aspects of field ionization of molecular states are still incompletely resolved. Obviously core structure adds to the complexity of the phenomenon, giving rise to processes such as forced ionization [26] or field-induced rotational autoionization [32–37].

In the present study on H_3 , complications related to autoionization are avoided because we concern ourselves with the Rydberg series that converge to the lowest rovibrational level of the electronic ground state of ortho-

H_3^+ . In addition, owing to the very large energy separations between the rotational and vibrational levels of H_3^+ , the mixing with core excited series is generally negligible except for specific interlopers [40].

Field ionization of Rydberg states of H_3 has been a primary tool to investigate photoabsorption to excited states of H_3 . In these studies, many unexpected intensity windows in the ionization efficiency have appeared and anomalous electric-field-dependent variations in the intensity of low- and high-Rydberg states have been noted [40–45]. The goal of the present study was to investigate in more detail the EFI properties of H_3 and their possible influence on the appearance of the absorption spectra of H_3 . This article discusses two observations that we consider of general interest (1) the dependence of the field-ionization process on the projection of the total angular momentum ($M_N=0$ or 1) onto the field axis, and (2) the apparent difference between the behavior of states produced in a near-zero field and subsequently exposed to an electric field and that of Stark states excited in a field of the same magnitude. The latter phenomenon, which has previously been described for atomic hydrogen [1,2,27], is related to the loss of the quantization axis in the absence of a well-defined external field and is largely independent of the properties of the H_3 molecule.

II. DESCRIPTION OF THE EXPERIMENT

A schematic diagram of the experimental setup [45] is given in Fig. 1. The H_3 molecules are produced as a fast neutral beam by charge exchange of mass-selected H_3^+ molecules of 1.5-keV energy in a cesium vapor. The resulting neutral beam is purged of residual ions by a small electric deflection field and contains only molecules in the long-lived rotationless level of the $\bar{B}2p^2A_2''$ state [41,46]. Nearly all of these molecules are also in the lowest vibrational level, and all spectra discussed here involve excita-

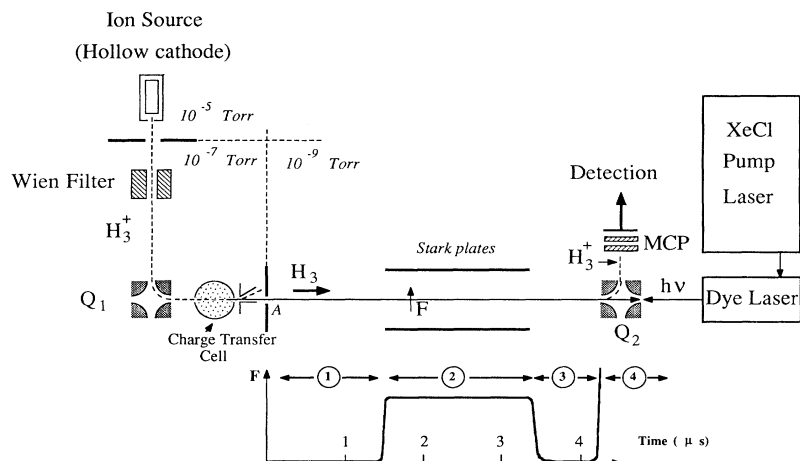


FIG. 1. Schematic of experimental setup. The fast H₃ neutral beam is collinearly excited by a tunable, pulsed laser beam. The neutral molecules that survive passage through the Stark-field region are field ionized at the entrance of the quadrupole deflector Q₂ and the resulting ions are detected during appropriate time gates corresponding to photoexcitation in region 1 or 2.

tion from the $N=0$, $K=0$, $v_1=v_2=0$ level. This state results from the addition of a $2p$ electron to the lowest rotational level of ortho-H₃⁺ ($N^+=1$, $K^+=0$). The neutral beam molecules are photoexcited in an ultrahigh vacuum chamber by a counterpropagating, pulsed dye laser beam [excimer pumped, unfocused 0.05–1 mJ/pulse, 0.15 cm⁻¹ (FWHM), *P*-terphenyl dye] along a 120-cm-long interaction region. A fixed ionizing field at the entrance of the energy analyzer, Q₂, is used for detecting those excited molecules that survive passage through the interaction region as neutral species. The magnitude of this detection field (2.3 kV/cm) is the same in all the experiments described here. Ions resulting from EFI in the detection field are separated by mass in the electrostatic quadrupole Q₂ and monitored by a microchannel plate detector.

During their path along the interaction region, the H₃ molecules successively traverse four regions of different electric fields. These regions are separated by transition zones where the field is not precisely defined but varies over a few centimeters, corresponding to transit times of about 100 ns. These four different regions (labeled 1 through 4 at the bottom of Fig. 1) can be described as follows.

Region 1 is a near-zero field region between aperture A and the Stark plates. Here the electric field is small (about 0.1 V/cm) and is mainly due to the motion of the neutral molecules in residual magnetic fields. At a beam energy of 1.5 keV, the motional electric field induced by the uncompensated magnetic field of the earth has a magnitude of 0.09 V/cm and is directed nearly parallel to the Stark field applied in region 2. Other small residual fields that are not precisely characterized exist in this region.

Region 2 has a well-defined transverse electric field (hereafter called the Stark field) that is defined by two parallel plates 45 cm long, 10 cm wide, and 2.44 cm apart. At a beam energy of 1.5 keV, H₃ molecules spend about 1.5 μs in this region. In region 2, one component of the motional electric field due to the earth's magnetic field can be compensated by the applied field. In a previ-

ous publication [45], we estimated that the lowest achievable value of the residual field in our experiment is on the order of 0.05 V/cm in region 2 and ~0.1 V/cm in region 1.

Region 3 is another field-free (near-zero field) region with the same properties as region 1.

Region 4 is a region of strong electric field at the entrance of Q₂ (the detection field) where the Rydberg molecules are ionized before being mass selected.

Since a pulsed laser is used to prepare the Rydberg states and since the molecules propagate through the interaction region with a velocity of 3×10^7 cm/s, we use the time of arrival of each ion to determine where along the interaction region the neutral precursor to the ion was photoexcited. Thus, with proper electronic gating (see time scale in Fig. 1), we can simultaneously record two distinct processes: (a) photoexcitation of states under near-zero-field conditions in region 1 followed by passage of the molecules through the Stark-field region, and (b) excitation of states in the Stark field.

In both cases, the Rydberg states that survive passage through the Stark field without being ionized reach the detection field (region 4), where they are field ionized for principal quantum numbers larger than $n \gtrsim 30$. Ions falling into the arrival time "windows" set by gates 1 and 2 are recorded to give a near-zero-field spectrum and a Stark spectrum, respectively. Ions formed in the Stark-field region are bent away from the neutral beam direction by the perpendicular field and thus are lost for the detection process. Consequently, EFI in the Stark-field region appears as a decrease in the detected ion signal.

We perform the identical experiment with atomic hydrogen or helium by simply changing the mass selection of the ion beam in the Wien filter from H₃⁺ to H⁺ or He⁺ and adjusting the electronic gating times for the detection. Charge exchange in cesium vapor produces neutral atoms in the H(2s) and the He(2s ¹S^o) states, and we use one-photon photoexcitation to produce either the Balmer series or the np ¹P^o series members from these states.

III. SUMMARY OF THE THEORY OF ELECTRIC-FIELD IONIZATION

A. Classical thresholds

In discussing our experimental spectra, it is useful to refer to three model thresholds that are often defined in EFI work: the saddle-point energy, the “red-state” diabatic threshold, and the “blue-state” diabatic threshold (see Fig. 2).

The saddle-point energy E_{SP} corresponds to the local maximum of the sum of the Coulomb and Stark potentials along the field axis. From a classical point of view, the states above this energy are in the continuum and therefore ionize. This classical threshold has a hydrogenic value of [12,47]

$$E_{\text{SP}} = -2\sqrt{F} + |m|F^{3/4} + \frac{3}{16}m^2F \approx -2\sqrt{F}, \quad (1)$$

where m is the projection of the electronic angular momentum along the field axis, F is the Stark field, and all quantities are given in atomic units (1 a.u. of electric-field strength is $5.142\,208\,2 \times 10^9$ V/cm). A zero-field state with effective principal quantum number n^* reaches the saddle-point energy at the threshold field:

$$F_{\text{sp}} = \frac{1}{16n^{*4}}. \quad (2)$$

The separation of the Schrödinger equation for atomic hydrogen in parabolic coordinates [3] leads to the introduction of the parabolic quantum numbers n_1 and n_2 ,

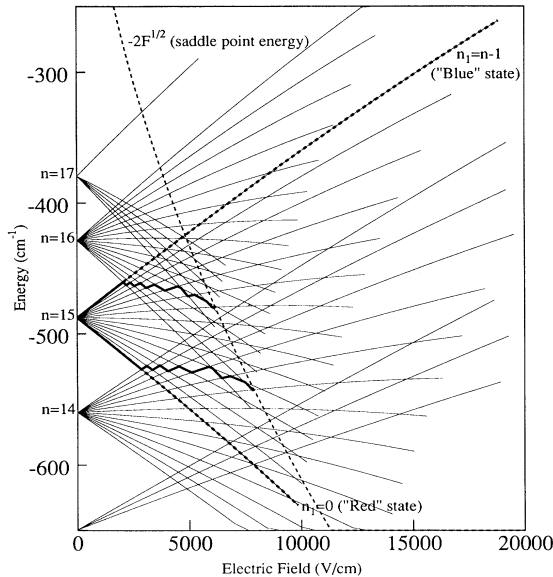


FIG. 2. Hydrogenic Stark map in the vicinity of $n=15$ ($m_l=0$). For each parabolic state $(n, n_1, m_l=0)$, the curve representing the energy as a function of the electric field ends when the ionization rate becomes larger than 10^6 s⁻¹. The dashed line labeled $-2F^{1/2}$ represents the position of the saddle-point energy. Bold solid lines show examples of adiabatic passage to ionization, while bold dashed lines give the limits of the diabatic passage from zero field to high field for the $(n=15, n_1=0)$ and $(n=15, n_1=14)$ states.

where $n_1 + n_2 + |m| + 1 = n$. In this framework it is possible to calculate the lifetime of each Stark sublevel (n_1, n_2) against field ionization. This lifetime decreases when n or F increases, whereas, for a given n manifold and a given field, lifetime and energy increase with n_1 .

In parabolic coordinates ($\xi=r+z$, $\eta=r-z$, r being the distance from the ion core to the electron position and z being the coordinate along the external electric-field axis) the effective potential along the ξ coordinate is always attractive while it passes over a local maximum before decreasing toward $-\infty$ along the η coordinate. The magnitude of this local maximum depends on the parabolic quantum numbers n_1 and n_2 and has been termed “critical energy” by Herrick [6]. It varies between the two limits defined below.

In first-order, the energy of the reddest member of the n manifold ($n_1=0$, $m=0$) in a field F is [3]

$$E_{(n_1=0, m=0)} = -\frac{1}{2n^2} - \frac{3}{2}n^2F. \quad (3)$$

The wave function of the red Stark state is mainly localized on the side of the saddle point, and therefore the red state should ionize when $E_{(n_1=0)} \approx -2\sqrt{F}$ and the approximate ionization field for the $n_1=0$ state is given by

$$F_r \approx \frac{1}{9n^4}. \quad (4)$$

This gives, for the zero-field energy of a state whose reddest Stark component ionizes at a given field value F ,

$$E_r \approx -\frac{3}{2}\sqrt{F}. \quad (5)$$

This value is referred to as the “red-state” diabatic threshold.

At very large principal quantum numbers, a variational calculation developed by Herrick [6] gives the field value for ionization of the bluest Stark component ($n_1=n-|m|-1$) as

$$F_b \approx \frac{32}{81n^4}. \quad (6)$$

Equation (6) predicts the zero-field energy of a state whose bluest Stark component ionizes at a specific electric-field value F as

$$E_b \approx -\frac{9}{8}\sqrt{F/2}. \quad (7)$$

This value is referred to as the “blue-state” diabatic threshold.

These various thresholds do not correspond to specific ionization rates. Rather, the onset of EFI near threshold is so rapid that the system can be considered stable below and unstable above these thresholds.

B. Results of quantum calculations

The quantum calculations do not predict an EFI threshold but instead a field-ionization rate. An effective threshold field can be defined once the observation time scale for the field-ionization process is specified. Damburg and Kolosov [7] developed a semiempirical formula for the ionization rates. Their treatment is based on the energy expression at the fourth order of the perturbation theory.

$$\begin{aligned}
E(n, n_1, n_2, m, F) = & -\frac{1}{2n^2} + \frac{3}{2}n(n_1 - n_2)F - \frac{n^4}{16}[17n^2 - 3(n_1 - n_2)^2 - 9m^2 + 19]F^2 \\
& + \frac{3}{32}n^7(n_1 - n_2)[23n^2 - (n_1 - n_2)^2 + 11m^2 + 39]F^3 \\
& - \left[\frac{n^{10}}{1024} \right] [5487n^4 + 35182n^2 - 1134m^2(n_1 - n_2)^2 \\
& + 1806n^2(n_1 - n_2)^2 - 3402n^2m^2 + 147(n_1 - n_2)^4 - 549m^4 \\
& + 5754(n_1 - n_2)^2 - 8622m^2 + 16211]F^4.
\end{aligned} \tag{8}$$

In an experiment, the effective “threshold” field is defined by the average time a molecule spends in the Stark-field region (in our case $\sim 10^{-6}$ s). In the vicinity of the critical field values [for the extreme Stark components these are defined by Eqs. (4) and (6)], the ionization rate varies by several orders of magnitude when the field is varied by only a few percent. As a consequence, near the critical field, effective thresholds and critical energies are similar within a few percent.

For hydrogenic ionization rates Damburg and Kosolov [7] have given the semiempirical formula given by

$$\begin{aligned}
\Gamma = & \frac{(4R)^{2n_2+m+1} e^{-2R/3}}{n^3 n_2! (n_2+m)!} \\
& \times \exp \left[-n^3 \frac{F}{4} (34n_2^2 + 34n_2m + 46n_2 + 7m^2 \right. \\
& \left. + 23m + \frac{53}{3}) \right],
\end{aligned} \tag{9}$$

where $R = (-2E)^{3/2}/F$ and E is the energy calculated from Eq. (8).

The relation between the energy and the field strength at the ionization threshold for a given n manifold depends primarily on the value of n_1 and to a lesser extent on m_l . The red state ($n_1=0$) has the lowest energy and the highest ionization rate, because its wave function has a high probability density near the saddle point. For an ionization rate of 10^6 s^{-1} , the approximate values of the critical field [Eq. (4)] and the critical energy [Eq. (5)] of the reddest state differ by only a few percent from the threshold values calculated using Eqs. (8) and (9). On the other hand, the bluest state ($n_1=n-|m|-1$) has the highest energy, but its wave function shows only a very small electron density near the saddle point and consequently its ionization rate is small. Numerical calculations show that, in the region of interest here ($50 < n < 100$), F_{blue} is two or three times larger than F_{red} for a given n manifold, consistent with the variational results [6] (4) and (6).

The hydrogenic Stark manifolds displayed in Fig. 2 have been computed from Eqs. (8) and (9). For each n and n_1 , the energy of the $m=0$ Stark level is plotted as a function of the electric field. Curves end at a field value where the ionization rate reaches 10^6 s^{-1} .

IV. EXPERIMENTAL RESULTS

Two types of spectra were examined using the apparatus shown in Fig. 1. One type is obtained by scanning the wavelength of the exciting laser; this spectrum is recorded for a fixed setting of the Stark field, the detection field, and the laser polarization. A second kind of spectrum is obtained by scanning the magnitude of the Stark field; it is recorded for a fixed setting of the excitation wavelength, the detection field, and the laser polarization. EFI thresholds appear in both spectra. An important point concerning the observed EFI thresholds is that, if a molecule is ionized in the Stark field, the ion is also deflected by the Stark field and thus never reaches our detector. Thus, in our spectra, contrary to the usual experiments, the ionization thresholds correspond to a decrease in the ion signal.

A. Threshold spectra of H_3

A typical set of wavelength-dependent spectra for H_3 is given in Fig. 3. These spectra are recorded with a field of

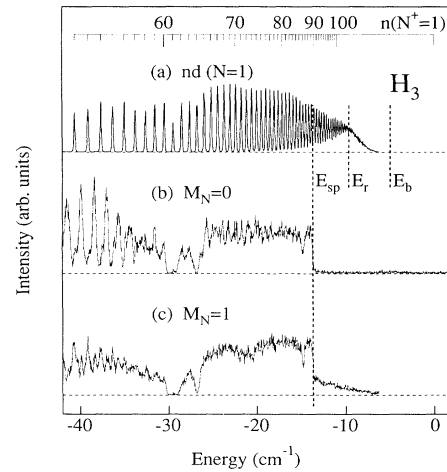


FIG. 3. Excitation spectra of H_3 with a Stark field of 5 V/cm for states excited in zero field (a), in the Stark field with $M_N=0$ (b), and in the field with $M_N=1$ (c). E_{sp} , E_r , and E_b indicate the positions of the saddle-point energy, the red-state ($n_1=0$) threshold, and the blue-state ($n_1=n-1$) threshold, respectively. Here and in the following figures, the energy scale origin is the lowest ionization limit of H_3 : $29\,562.58 \text{ cm}^{-1}$ above the metastable state.

5 V/cm applied in the Stark region. In the top spectrum (a), the molecules are excited in region 1 (near-zero field) and then enter the Stark-field region. This spectrum shows the excitation of the nd ($N=1$) Rydberg series that converges to the lowest ortho level of H_3^+ ($N^+=1$, $K^+=0$). This limit lies $29\,562.58\text{ cm}^{-1}$ above the initial metastable state and is used as the origin of the energy scale given. A significant decrease in the ion signal is observed for n values greater than 106, and no Rydberg molecules with quantum numbers exceeding 140 are found to reach the detector. The conclusion is that the higher n members are field ionized in the Stark field and hence prevented from reaching the detection field. No sharply defined ionization threshold exists in this case where the states are excited prior to the ionizing field. The model thresholds calculated for 5 V/cm are indicated in the figure. We see that the states lying between E_r and E_b , well above the saddle-point energy E_{SP} , are stable on the time scale required to traverse the Stark field ($\sim 1\ \mu\text{s}$).

A generally different picture emerges when excitation occurs in the Stark-field region (region 2), as is evident in traces (b) and (c) in Fig. 3. Rather well-defined thresholds appear in these two spectra near $n=90$, the predicted saddle-point energy for a field of 5 V/cm. The projection of the total angular momentum of the molecule (neglecting spins) onto the field axis, M_N , is the only quantum number conserved in the field. In the metastable state, $M_N=N=0$. Thus, depending on the orientation of the laser polarization with respect to the Stark field, we can excite states with $M_N=0$ ($\mathbf{E}_{\text{laser}}\parallel\mathbf{E}_{\text{Stark}}$, center spectrum in Fig. 3) or $M_N=\pm 1$ ($\mathbf{E}_{\text{laser}}\perp\mathbf{E}_{\text{Stark}}$, bottom spectrum in Fig. 3). In the following, we use the notation $M_N=1$ instead of $M_N=\pm 1$.

We see that the $M_N=0$ spectrum exhibits a distinct threshold at the zero-field energy of the $90d$ state, with practically all $M_N=0$ states being ionized above the classical threshold E_{SP} . In the $M_N=1$ spectrum, we again observe a sharp decrease in the ion signal at the saddle-point energy; however, a significant proportion of the states are observed to be stable above this threshold.

These differences are also apparent from Figs. 4 and 5, which show the results for Stark-field values ranging from 0 to 10 V/cm. Figure 4 gives spectra obtained by exciting in the near-zero field and then subjecting the Rydberg states to the Stark field indicated. The model thresholds are shown by arrows, and we see that EFI becomes gradually complete between E_r and E_b when the states are prepared at near-zero-field conditions. Spectra recorded with atomic helium under identical conditions give results basically identical to those in Fig. 4. Figures 5(a) and 5(b) correspond to excitation in the Stark field for $M_N=0$ and 1, respectively. The arrows represent the position of the saddle-point energy. For each field value, it is clear that ionization is nearly 100% efficient above the saddle-point energy when $M_N=0$ but less complete (varying from 60% for $F=2$ V/cm to 80% for $F=10$ V/cm when $M_N=1$).

We can look at EFI in finer detail by using the second technique described above, namely, exciting a Rydberg state at a given photon energy and then measuring the

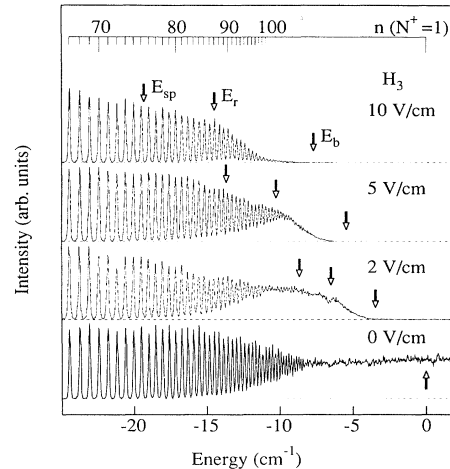


FIG. 4. H₃ Rydberg spectra when the molecules are excited in a near-zero field and then exposed to a Stark field. Arrows indicate the saddle-point energy and the red-state and blue-state diatomic thresholds. Field ionization occurs between E_r and E_b , well above E_{SP} .

remaining ion signal as a function of the magnitude of the Stark field. Figure 6 shows such spectra at a wavelength corresponding to excitation of the field-free $70d$ ($N=1$) state. The upper spectrum refers to excitation at zero field, prior to the interaction with the Stark field. The bold dashed line is a hydrogenic simulation based on Eqs. (8) and (9). A small portion (about a quarter) of the molecules are found to be field ionized just above F_{SP} , but ionization only gradually reaches completion above the red-state threshold. The blue-state threshold field for $n=70$ lies at ~ 85 V/cm, outside the field scale shown in Fig. 6. The lower spectrum in Fig. 6 corresponds to states excited in the field for $M_N=0$. Obviously ionization is complete above F_{SP} for $M_N=0$ states excited in the field.

B. Threshold spectra of atomic hydrogen

Several aspects of the ionization phenomena described so far become clearer in the context of atomic hydrogen, for which exact calculations are available. We show in Figs. 7 and 8 spectra for atomic hydrogen recorded under conditions identical to those used for H₃ in Figs. 3 and 6, respectively. In the top spectrum in Fig. 7, the Balmer series $np\leftarrow 2s$ is excited in the near-zero field and subsequently the atoms traverse the Stark-field region, where a field of 5 V/cm is applied. We see that the ion signal decreases only gradually between the thresholds E_r and E_b , quite analogous to the results for H₃ in the uppermost spectrum of Fig. 3. The lower spectrum in Fig. 7 corresponds to atomic hydrogen being excited in a field of 5 V/cm with the laser polarization perpendicular to the Stark field ($m_l=1$). This spectrum is quite different from the analogous spectrum for triatomic hydrogen in Fig. 3. In atomic hydrogen, the threshold region spreads from the saddle-point energy E_{SP} (where $n_1=0$ states are ionized) all the way to the ionization limit (where states with $n_1\approx n$ are ionized). In Fig. 7 (bottom), the thin trace gives the experimental spectrum and the bold trace the

result of a hydrogenic calculation which shows the high degree of reliability of the hydrogenic theory [Eqs. (8) and (9)].

A similar difference is apparent in Fig. 8, which gives fixed-wavelength spectra for excitation of H ($n = 70$) that can be compared with those shown in Fig. 6 for H₃. The dashed line in Fig. 8 (top) gives the result of a hydrogenic simulation which fits almost perfectly the experimental spectrum.

V. DISCUSSION

The field-ionization properties of the Stark states of nonhydrogenic systems depend on the strength of the mixing between pure parabolic states of different n value and the dynamics at the avoided crossings between these states. However, this mixing alone is not sufficient to explain the hydrogenic behavior of H₃ states excited in the region of near-zero field, as will be detailed in Sec. V B. Section V C gives a qualitative explanation of the

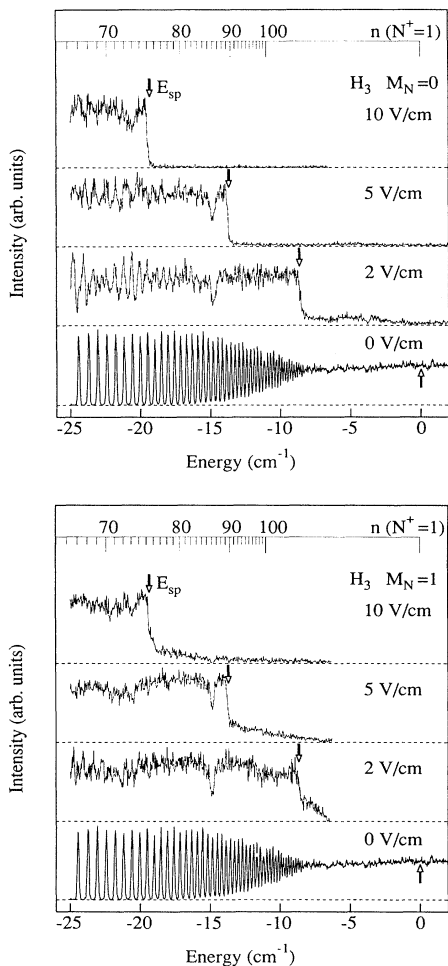


FIG. 5. Stark spectra of H₃ for different field values (0–10 V/cm) and $M_N=0$ (a) or $M_N=1$ (b). The arrows indicate the saddle-point energy. The spectra clearly show a sharp decrease in the signal at E_{SP} as well as the stability of part of the $M_N=1$ states above this threshold.

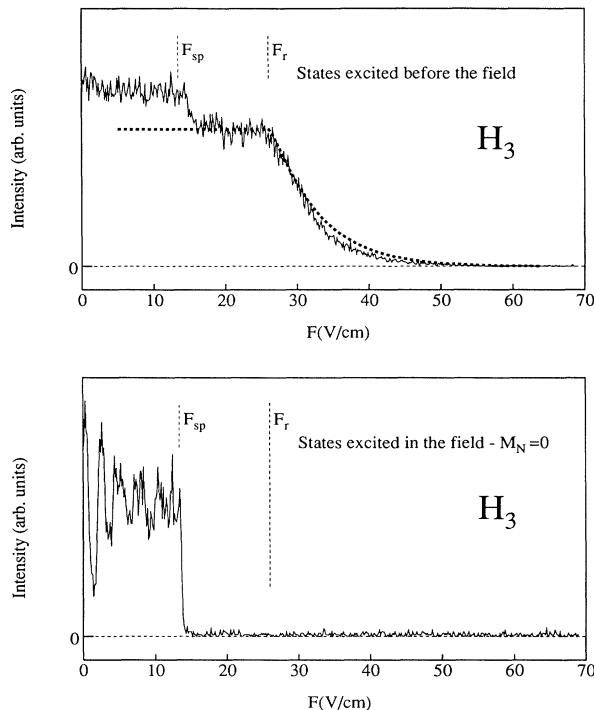


FIG. 6. H₃⁺ signal as a function of field strength after excitation of H₃ molecules at the energy of the 70d ($N=1$) state with excitation in the near-zero field (top) or in the Stark field (bottom). The bold dashed line (top spectrum) is a hydrogenic simulation (see text). The top spectrum shows that about 25% of the molecules are ionized just above the saddle-point energy, i.e., at the field strength F_{SP} , where the energy of the 70d state equals the saddle-point energy.

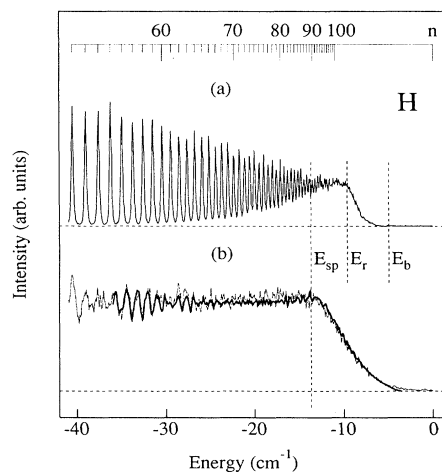


FIG. 7. Excitation spectra of atomic hydrogen with a Stark field of 5 V/cm for states excited in near-zero field (a) and in the Stark field with $m_l=1$ (b) (thin line: experiment, bold line: calculation). Compare with the spectra of Fig. 3 to see the nonhydrogenic behavior of H₃ when excited in the Stark field and its hydrogenic behavior when excited in the zero field.

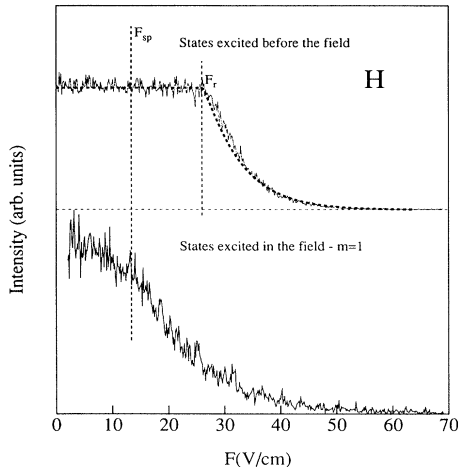


FIG. 8. Same as Fig. 6 but for atomic hydrogen. The excitation takes place at the energy of the $70p$ state in the zero field (top) and in the Stark field (bottom), with $m_l=1$. The bold dashed line (top spectrum) is a hydrogenic simulation assuming $m_l=1$ and an ionization rate of 10^6 s^{-1} .

different EFI processes observed for $M_N=0$ and $M_N=1$ series. Unlike the previous point, this one is a consequence of particular characteristics of H₃. Finally, we analyze the dynamic evolution of states that are excited in the near-zero field and then subjected to the Stark field.

A. Adiabaticity and diabaticity

In the nonrelativistic approximation, the Stark levels from different n manifolds of atomic hydrogen are strictly uncoupled. In the nonhydrogenic case, however, the Stark states cannot be described by purely parabolic $|n_1, n_2, m\rangle$ wave functions and the crossings between the Stark states are avoided. The coupling among different $|n_1, n_2, m\rangle$ states of different n value determines the dynamic path along which the Stark states evolve in a time-varying electric field, and two extreme cases can be distinguished.

If the electric field is increased gradually, such that the mixing between the various n_1, n_2 components has time to be established, then a specific state will evolve along the adiabatic path. For example, if the zero-field excited state was an nlm state, then the path followed toward ionization is such that the energy of the system is forced to stay between the zero-field energy of the $n-1$ and $n+1$ states because all crossings are avoided. In this case, the experimental ionization threshold follows rather closely the classical formula $1/16n^{*4}$, where n^* , the effective principal quantum number at ionization, differs at most by about 0.5 from the original n value [32]. This is why the saddle-point threshold is sometimes referred to as the adiabatic threshold. Ionization can occur in the vicinity of the saddle-point energy because there is always mixing with a rapidly ionized “red” component from a higher n manifold.

On the other hand, if the field is increased very rapidly, the avoided crossings may be traversed diabatically and a zero-field state could follow along any of the paths be-

tween the “red” ($n_l=0$) state and the “blue” ($n_l=n-|m|-1$) state from zero field to ionization. As a consequence, we would expect to observe a gradual ionization of the different Stark sublevels at field values between F_{red} and F_{blue} . This difference is indicated in Fig. 2, where the bold tracks give examples of adiabatic passage to ionization whereas the thin lines are examples of diabatic passage.

Direct evidence for both adiabatic and diabatic behavior is apparent in the upper trace in Fig. 6. Some H₃ molecules (about 25%) are observed to ionize near the saddle-point energy, while the remainder show a field dependence similar to that seen for atomic hydrogen (compare with top curve in Fig. 8). To explain this observation we first have to characterize the nature of states excited in region 1.

B. Properties of the “zero-field” states

States that are photoexcited in region 1 are not prepared under truly zero-field conditions, but they are formed in a region of ill-determined residual fields whose direction and magnitude is not constant along the beam path. A main component of this field comes from the motional electric field that results from the earth’s magnetic field ($\leq 100 \text{ mV/cm}$). When optical excitation occurs under such conditions, then at time $t=0$ an $M_N=0$ or 1 state will be excited because the initial state has $N=M_N=0$. At the time of excitation, the quantization axis is defined by the local field. However, this quantization axis will be lost during the passage from the point of excitation to the region of the Stark field, and the total angular momentum N of the molecule will precess around the random directions of the residual field. This would be true even if the field was as close as possible to zero [1,2,27]. However, if the electric field was really negligible, the accessible values of M_N would fall into the range from 0 to ± 3 , owing to the low values of the core kinetic momentum ($N^+=1$) and the electronic angular momentum ($l=0$ or 2) that can be prepared from our initial state of H₃.

To explain the EFI behavior in the upper curve in Fig. 6, we first consider the result of a perturbative calculation [45] for the oscillator strength of the Stark states belonging to the $n=70$ manifold. The calculation used the quantum defects listed in Table I. Figure 9 gives these results for $M_N=0$ and 1 at $F=0.1 \text{ V/cm}$. Calculated intensities have been normalized so that the sum of the line intensities for a given n manifold is 1. Two results from

TABLE I. Quantum defects used in our calculations.

Orbital symmetry	Quantum defects	Reference
s	0.07	[45]
pa''	0.05	[43]
pe'	0.39	[43]
d	0.02	[41]
f	0.01	[42]
$l > 3$	0.00	

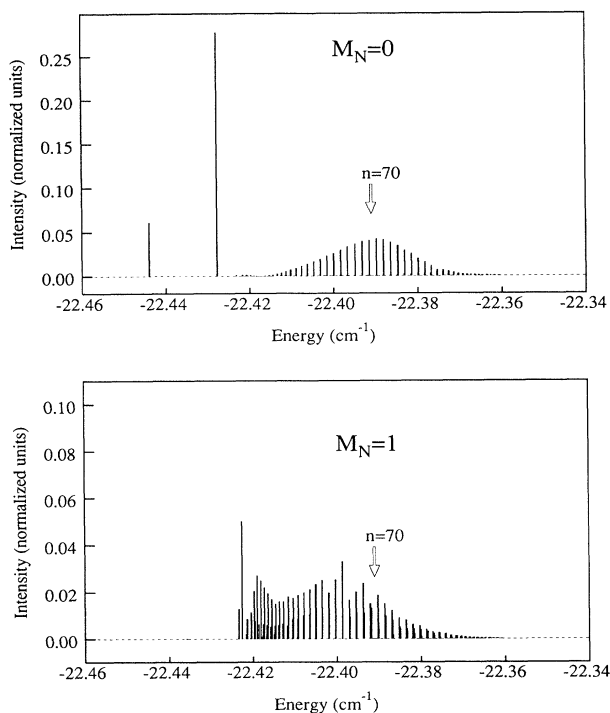


FIG. 9. Perturbative calculation of the oscillator strength for the $n=70$ manifold of H_3 in a field $F=0.1$ V/cm. The top spectrum shows results for $M_N=0$ and the bottom spectrum for $M_N=1$.

Fig. 9 are important for the discussion of the ionization behavior seen in Fig. 6.

(1) The energy spread of the $n=70$ Stark manifold at an electric-field strength of 0.1 V/cm is $\lesssim 0.08$ cm^{-1} . Our experimental resolution is given by the laser bandwidth ($\lesssim 0.15$ cm^{-1}). Thus the laser will excite all the components of the manifold under the conditions that apply to the top spectrum of Fig. 6.

(2) The intensity of each unresolved Stark component is approximately proportional to the square of its d ($l=2$) character. The oscillator strengths show that the intensity is distributed over the entire manifold. The strongest line bears 27% of the total oscillator strength for $M_N=0$ and 5% for $M_N=1$. The intense transitions on the red side of the manifolds correspond to the states that correlate to the nd states at the zero-field limit. More generally, all the lines on the red side of $n=70$ correlate to states with a positive quantum defect in zero field, that is, with low- l states ($l < 3$), while the lines between -22.42 and -22.36 cm^{-1} correspond to the hydrogenic complex ($\mu \sim 0$) of high- l states.

In our calculation, the quantum defects are nonzero for $l \leq 3$, which corresponds to the ten lowest states of the manifold for $M_N=0$ (the nine lowest for $M_N=1$). The sum of the line intensities of these Stark states is 0.341 for $M_N=0$ and 0.078 for $M_N=1$. When these data are combined with a 1:2 statistical branching ratio for $M_N=0$ and $M_N=1$, this leads to a total of $(0.341 \times \frac{1}{3} + 0.078 \times \frac{2}{3}) \sim 17\%$ of the intensity going into

low- l components when broadband excitation occurs at 0.1 V/cm. This information can now be used to estimate the composition of states that enter the Stark-field region under the conditions of Fig. 6: For a given l value, the total angular momentum N with $N^+ = 1$ may take any value from 0 to l , and so does $|M_N|$. If we assume an equal partitioning of all the M_N values for each N subset (this is strictly true only if no quantization axis exists), the probability that an excited molecule is in a low- M_N state (say, $|M_N| < 3$) is 0.17 (the 17% corresponding to the low- l components) plus ~ 0.05 (the proportion of low M_N for high- l : high- N states $\sim 3:70$). In other words, only about 22% of the molecules excited in region 1 enter the Stark region with $|M_N| < 3$.

The experimental results in Figs. 5(a) and 5(b) suggest that, for $n=70$, about 100% of the $M_N=0$ states and about 80% of the $M_N=1$ states will be field ionized above E_{SP} when a field of ~ 13 V/cm (value of F_{SP} from $n=70$) is applied. Similarly, we can assume that a significant proportion of $M_N=2$ states are also ionized, but states with high M_N should behave purely hydrogenically, since no states with significant quantum defects participate in the $M_N > 2$ manifolds.

The above considerations suggest that about 22% of the excited molecules should ionize at the saddle-point energy or in its vicinity (depending on which adiabatic path they follow, E_{SP} may correspond to an effective $n^* = n \pm \frac{1}{2}$), while the remaining 78% of the molecules should ionize hydrogenically. This result fits almost perfectly the top spectrum in Fig. 6, where we see that about 25% of the molecules excited in the $n=70$ manifold in region 1 are field ionized just above F_{SP} while the remaining signal follows rather precisely the hydrogenic simulation shown by the dashed line (see also the experimental results for atomic hydrogen in Fig. 8). We observed rather similar behavior in experiments in atomic helium, and it is obvious from the above discussion that such behavior should be observed whenever the laser bandwidth encompasses the entire Stark manifold.

C. Influence of M_N on the electric-field ionization process

In Figs. 3 and 5, we note a difference in the behavior of the $M_N=0$ and $M_N=1$ Stark states. A significant proportion of $M_N=1$ states are stable, on the time scale of about 1 μs , above the saddle-point energy while nearly all $M_N=0$ states ionize within this time frame. The fraction of M_N states that are “stable” decreases as the field strength increases. For $M_N=1$, almost 40% of the molecules are stable above E_{SP} , when $F=2$ V/cm. This fraction decreases to 30 at $F=5$ V/cm, and to 20% at $F=10$ V/cm. For $M_N=0$, the fraction is 15% at $F=2$ V/cm, less than 5% at $F=5$ V/cm, and not measurable at $F=10$ V/cm. According to Eq. (2), these field values for E_{SP} correspond n_{SP}^* (values of the effective quantum number at the saddle point) of 113, 90, and 75, respectively. Below, we attempt to explain the difference in the $M_N=0$ and 1 spectra by using the results from a perturbative description of the Stark manifold of H_3 .

While a calculation for such large values of n is quite straightforward, we considered such an exercise out of proportion to our purpose and unnecessarily complicating owing to the very large number of Stark states involved at high n values. For reasons of clarity, we chose to examine the Stark manifolds for $n=19$ and 20. The results for these states should contain the essence of what is important for the higher n values, and they can be scaled to the case for the higher values. Figures 10 and 11 exhibit the Stark states predicted by the perturbative theory in the region of the crossing between the $n=19$ and 20 manifolds for $M_N=0$ (Fig. 10) and $M_N=1$ (Fig. 11). The Stark maps appear to be similar, but they reveal significant differences between the two cases.

For $M_N=0$, some avoided crossings are large (>0.1 cm^{-1}) and some nearly negligible (<0.01 cm^{-1}). Examination of a particular state from low field strength into the crossing region shows that it is always part of an ensemble of three states which never get closer than ~ 0.1 cm^{-1} to any other triplet. This feature is particularly apparent in the close-up view shown in the lower part of Fig. 10. Sets of three sublevels exist because the $N^+=1$ value of the core kinetic momentum gives rise to three components for each (n_1, n_2) state that correspond [45] to the three orientations of N^+ in the relation $\mathbf{N}=1+\mathbf{N}^+$, despite the fact that N and l are not well-defined quantum numbers in the presence of the field. We note from the

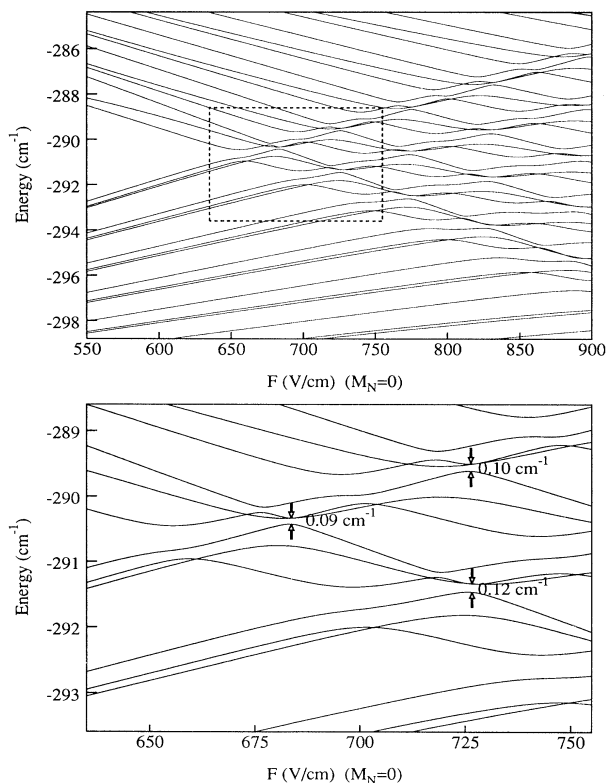


FIG. 10. Stark map of H_3 , $M_N=0$, showing the region of the crossing between the $n=19$ and $n=20$ manifolds (top) and details of the area within the dashed rectangle (bottom). Arrows in the bottom figure indicate the largest avoided crossings (see text).

manifold shown in the top part of Fig. 10 that this triplet character persists up into the high-field region.

For $M_N=1$ (Fig. 11), particular levels cannot be uniquely grouped into triplets once they reach the region of n mixing. One member of each triplet develops along a diabatic path as F increases. Such paths are indicated by a dashed arrow in the detail of Fig. 11. The calculation shows that these diabatic states have negligible s and p character ($\sim 10^{-4}$ for $n \approx 20$) while they possess a significant d component (0.1–0.2 for $n \approx 20$). We also conclude from the examination of the results of the perturbative calculation that these diabatic states bear about one-third of the total oscillator strength. We attribute the appearance of stable states above the saddle point in Fig. 5(b) to the existence of these diabatic components of the Stark manifold.

As a further difference to the $M_N=0$ case in Fig. 10, the adiabatic components of the $M_N=1$ manifold show generally smaller avoided crossings than those for $M_N=0$ (by about one order of magnitude). For atomic species, it is well known that the hydrogenic character becomes more pronounced as m_l increases, because of the diminution of the quantum defect with l . In the atomic case, a given m_l manifold includes only those states that have $l > m_l$. It is not clear *a priori* that the same situation exists in a molecular system, where the good quantum number M_N (m_l is not defined) does not formally impose a restriction on the value of l . Hence, the origin of the weak-

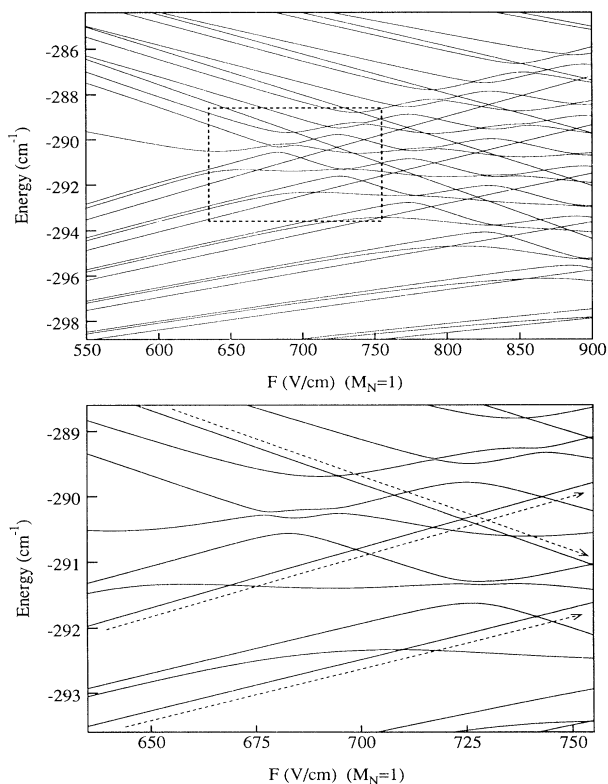


FIG. 11. Same as Fig. 10 but for the case $M_N=1$. Long dashed arrows underline the paths followed by the “diabatic” component of the Stark manifold.

er couplings occurring among the $M_N=1$ states is not obvious *a priori*. Inspection of the perturbation basis for $M_N=0$ and 1 shows that their only difference is the absence of the $(np, N=0)$ element in the $\{M_N=1\}$ basis. Experiments described in Ref. [40] show that the $(np, N=0)$ state is a strong mediator between the s and d states.

The lack of the $(np, N=0)$ element in the $M_N=1$ case therefore appears to lead to a diminution of the coupling, and we consider this lack to be the origin of the different behavior of states above the saddle-point energy. The width of the avoided crossings is a measure of the strength of the couplings between states from neighboring n manifolds and hence also of the importance of the mixing between these states. A comparison of Figs. 10 and 11 therefore suggests that the $M_N=0$ manifolds are more strongly coupled and mixed than the $M_N=1$ states. The magnitude of the avoided crossings suggests that this difference is about one order of magnitude. This difference is a particular characteristic of H_3 .

D. Dynamic evolution of Stark states

The results of the perturbative calculation presented in Figs. 10 and 11 can be used to analyze the dynamic evolution of states that are excited in a near-zero field and then subjected to a Stark field. We choose the example of Fig. 6 (top spectrum), where molecules are first excited to $n=70$ in a near-zero field and then enter (in about 100 ns) the Stark-field region. We examine the dynamic path followed by the $M_N=0$ and $M_N=1$ components. To apply the results in Figs. 10 and 11, we extrapolate these calculations to $n \sim 70$. The matrix elements of the Stark Hamiltonian between two neighboring states are proportional [45] to n^2F . The field strength corresponding to the onset of n mixing is $F_c = (3n^5)^{-1}$ (in a.u.). Hence, in the region of the avoided crossings, Stark Hamiltonian matrix elements between adjacent states are proportional to n^{-3} . The width of the avoided crossings is directly proportional to these matrix elements. Therefore the width of the avoided crossings for $n=70$ should be about $(\frac{70}{20})^3$ times smaller than that for $n=20$. In the $n=70$ manifold, the width of the large avoided crossings between each triplet will be of the order of $2 \times 10^{-3} \text{ cm}^{-1}$ for $M_N=0$ and $2 \times 10^{-4} \text{ cm}^{-1}$ for $M_N=1$. Using the Landau-Zener formula [48], we next calculate the probability for the system to jump from a diabatic state 0 to a diabatic state 1 at the crossing

$$P_{01} \approx \exp - \left[\frac{\eta_{01}}{v} \right], \quad (10)$$

where

$$\eta_{01} = \frac{\frac{2\pi}{\hbar} V_{01}^2}{\left| \frac{\partial E_1}{\partial F} - \frac{\partial E_0}{\partial F} \right|}$$

and

$$v = \frac{\partial F}{\partial t}.$$

E_0 and E_1 are the Stark energies of states 0 and 1, and V_{01} is the matrix element between the two states (one-half of the width of the avoided crossing). For the extreme members of two neighboring manifolds $[(n, n_1 \sim n)$ and $(n+1, n_1 \sim 0)]$ and for the values $n=70$, $F=10 \text{ V/cm}$, $\Delta t=100 \text{ ns}$, Eq. (10) leads to

$$1 - P_{01} = \begin{cases} 2 \times 10^{-2} & (\text{for } M_N=0) \\ 2 \times 10^{-4} & (\text{for } M_N=1) \end{cases}.$$

The number of large avoided crossings that a given state encounters is on the order of (nF_{SP}/F_c) , which is about $(3n^2/16)$. Under the (very crude) assumption that P_{01} is of similar magnitude at each crossing, the total probability that the system remains in the same diabatic state when F is increased from 0 to F_{SP} is about

$$P_{01}^{\text{tot}} = (P_{01})^{3n^2/16}. \quad (11)$$

In the present case this gives

$$P_{01}^{\text{tot}} \approx \begin{cases} 0 & (\text{for } M_N=0) \\ 0.83 & (\text{for } M_N=1) \end{cases}.$$

We conclude that under our experimental conditions the evolution of the $M_N=0$ components is globally adiabatic while the evolution of the $M_N=1$ components is mainly diabatic. This discussion also shows that diabaticity and hydrogenic behavior are far from synonymous.

VI. CONCLUSIONS

Ionization of high-Rydberg states of triatomic hydrogen in an external electric field has been investigated. The experimental results have demonstrated a fundamentally different behavior between states prepared in the electric field and those prepared prior to application of the electric field. A significant difference in character between the $M_N=1$ states and the $M_N=0$ states has been found. Both results have been discussed in the framework of a perturbative treatment of the Stark effect. The first aspect has been shown to be a rather general consequence of the lack of a durable quantization axis in a near-zero-field region. The second point is related to the weaker couplings that exist between the $M_N=1$ series members and it results mainly from the absence of the np ($N=0$) component in the $M_N=1$ manifold.

ACKNOWLEDGMENTS

This research was supported by the National Science Foundation under Grant No. PHY 87-06332 and by the Air Force Systems Command under Contract No. F 33615-90-C-2007. One of us (C.B.) wishes to thank NATO and CNRS for partial support.

- *Permanent address: Laboratoire de Spectrométrie Ionique et Moléculaire, Université Lyon I, Bâtiment 205, 43 Boulevard du 11 Novembre 1918, 69622 Villeurbanne CEDEX, France.
- [1] J. E. Bayfield and P. M. Koch, *Phys. Rev. Lett.* **33**, 258 (1974).
- [2] P. M. Koch and D. R. Mariani, *Phys. Rev. Lett.* **46**, 1275 (1981).
- [3] H. A. Bethe and E. E. Salpeter, *Quantum Mechanics of One- and Two-Electron Atoms* (Plenum, New York, 1977).
- [4] D. S. Bailey, J. R. Hiskes, and A. C. Riviere, *Nucl. Fusion* **5**, 41 (1965).
- [5] M. H. Rice and R. H. Good, Jr., *J. Opt. Soc. Am.* **52**, 239 (1962).
- [6] D. R. Herrick, *J. Chem. Phys.* **65**, 3529 (1976).
- [7] R. J. Damburg and V. V. Kolosov, *J. Phys. B* **9**, 3149 (1976); **11**, 1921 (1978); **12**, 2637 (1979).
- [8] D. Banks and J. G. Leopold, *J. Phys. B* **11**, 37 (1978).
- [9] H. J. Silverstone, *Phys. Rev. A* **18**, 1853 (1978).
- [10] H. J. Silverstone, B. G. Adams, J. Cizek, and P. Otto, *Phys. Rev. Lett.* **43**, 1498 (1979).
- [11] E. Luc-Koenig and A. Bachelier, *J. Phys. B* **13**, 1743 (1980); **13**, 1769 (1980).
- [12] M. L. Zimmerman, M. G. Littman, M. M. Kash, and D. Kleppner, *Phys. Rev. A* **20**, 2251 (1979).
- [13] D. Kleppner, M. G. Littman, and M. L. Zimmerman, in *Rydberg States of Atoms and Molecules*, edited by R. F. Stebbings and F. B. Dunning (Cambridge University Press, Cambridge, England, 1983); M. G. Littman, M. M. Kash, and D. Kleppner, *Phys. Rev. Lett.* **41**, 103 (1978).
- [14] T. W. Ducas, M. G. Littman, R. R. Freeman, and D. Kleppner, *Phys. Rev. Lett.* **35**, 366 (1975).
- [15] D. Tuan, S. Liberman, and J. Pinard, *Opt. Commun.* **18**, 533 (1976).
- [16] T. F. Gallagher, L. M. Humphrey, R. M. Hill, and S. M. Edelstein, *Phys. Rev. Lett.* **37**, 1465 (1976).
- [17] C. Fabre, P. Goy, and S. Haroche, *J. Phys. B* **10**, L183 (1977).
- [18] T. F. Gallagher, L. M. Humphrey, W. E. Cooke, R. M. Hill, and S. A. Edelstein, *Phys. Rev. A* **16**, 1098 (1977).
- [19] J. L. Vialle and H. T. Duong, *J. Phys. B* **12**, 1407 (1979).
- [20] T. H. Jeys, G. W. Foltz, K. A. Smith, E. J. Beiting, F. G. Kellert, F. B. Dunning, and R. F. Stebbings, *Phys. Rev. Lett.* **44**, 390 (1980).
- [21] F. G. Kellert, T. H. Jeys, G. B. McMillian, K. A. Smith, F. B. Dunning, and R. F. Stebbings, *Phys. Rev. A* **23**, 1127 (1981).
- [22] T. H. Jeys, G. B. McMillian, K. A. Smith, F. B. Dunning, and R. F. Stebbings, *Phys. Rev. A* **26**, 335 (1982).
- [23] F. B. Dunning and R. F. Stebbings, in *Rydberg States of Atoms and Molecules* (Ref. [13]).
- [24] S. Feneuille, S. Liberman, J. Pinard, and A. Taleb, *Phys. Rev. Lett.* **42**, 1406 (1979).
- [25] S. Liberman and J. Pinard, *Phys. Rev. A* **20**, 507 (1979).
- [26] W. Sandner, K. A. Safinya, and T. F. Gallagher, *Phys. Rev. A* **33**, 1008 (1986).
- [27] W. Van der Water, D. R. Mariani, and P. M. Koch, *Phys. Rev. A* **30**, 2399 (1984).
- [28] R. F. Stebbings, C. J. Lattimer, W. P. West, F. P. Dunning, and T. B. Cooke, *Phys. Rev. A* **20**, 2251 (1979).
- [29] C. F. Barnett, J. A. Ray, and A. Russek, *Phys. Rev. A* **5**, 2110 (1972).
- [30] T. J. Morgan, C. F. Barnett, J. A. Ray, and A. Russek, *Phys. Rev. A* **20**, 1062 (1979).
- [31] R. Kachru and H. Helm, *Phys. Rev. Lett.* **55**, 1575 (1985).
- [32] E. Y. Xu, H. Helm, and R. Kachru, *Phys. Rev. Lett.* **59**, 1096 (1987).
- [33] C. R. Mahon, G. R. Janik, and T. F. Gallagher, *Phys. Rev. A* **41**, 3746 (1990).
- [34] D. Eisel and W. Demtröder, *Chem. Phys. Lett.* **88**, 481 (1982).
- [35] G. R. Janik, O. C. Mullins, C. R. Mahon, and T. F. Gallagher, *Phys. Rev. A* **35**, 2345 (1987).
- [36] C. Bordas, M. Broyer, P. Labastie, and B. Tribollet, in *Photophysics and Photochemistry Above 6 eV*, edited by F. Lahmani (Elsevier, Amsterdam, 1985).
- [37] C. Bordas, P. Brevet, M. Broyer, J. Chevalyere, and P. Labastie, *Europhys. Lett.* **3**, 789 (1987).
- [38] E. D. Poliakoff, J. L. Dehmer, A. C. Parr, and G. E. Leroi, *Chem. Phys. Lett.* **111**, 128 (1984).
- [39] M. A. Duncan, T. G. Dietz, and H. E. Smalley, *J. Chem. Phys.* **75**, 2118 (1981).
- [40] C. Bordas and H. Helm, *Phys. Rev. A* **43**, 3645 (1991).
- [41] H. Helm, *Phys. Rev. Lett.* **56**, 42 (1986); *Phys. Rev. A* **38**, 3425 (1988).
- [42] L. J. Lembo, C. Bordas, and H. Helm, *Phys. Rev. A* **42**, 6660 (1990).
- [43] C. Bordas, L. J. Lembo, and H. Helm, *Phys. Rev. A* **44**, 1817 (1991).
- [44] A. Dodhy, W. Ketterle, H.-P. Messmer, and H. Walther, *Chem. Phys. Lett.* **151**, 133 (1988).
- [45] C. Bordas and H. Helm, *Phys. Rev. A* **45**, 387 (1992).
- [46] G. I. Gellene and R. F. Porter, *J. Chem. Phys.* **93**, 6303 (1990).
- [47] W. E. Cooke and T. F. Gallagher, *Phys. Rev. A* **17**, 1226 (1978).
- [48] *Atomic and Molecular Processes*, edited by D. R. Bates (Academic, New York, 1962).